

NUCLEOSYNTHESIS IN TYPE IA SUPERNOVAE

K. Nomoto^a, K. Iwamoto^a, N. Nakasato^a, F.-K. Thielemann^b,
F. Brachwitz^b, T. Tsujimoto^c, Y. Kubo^a, N. Kishimoto^a

^aDepartment of Astronomy, University of Tokyo, Tokyo 113

^bInstitut für Theoretische Physik, Universität Basel CH-4056 Basel, Switzerland

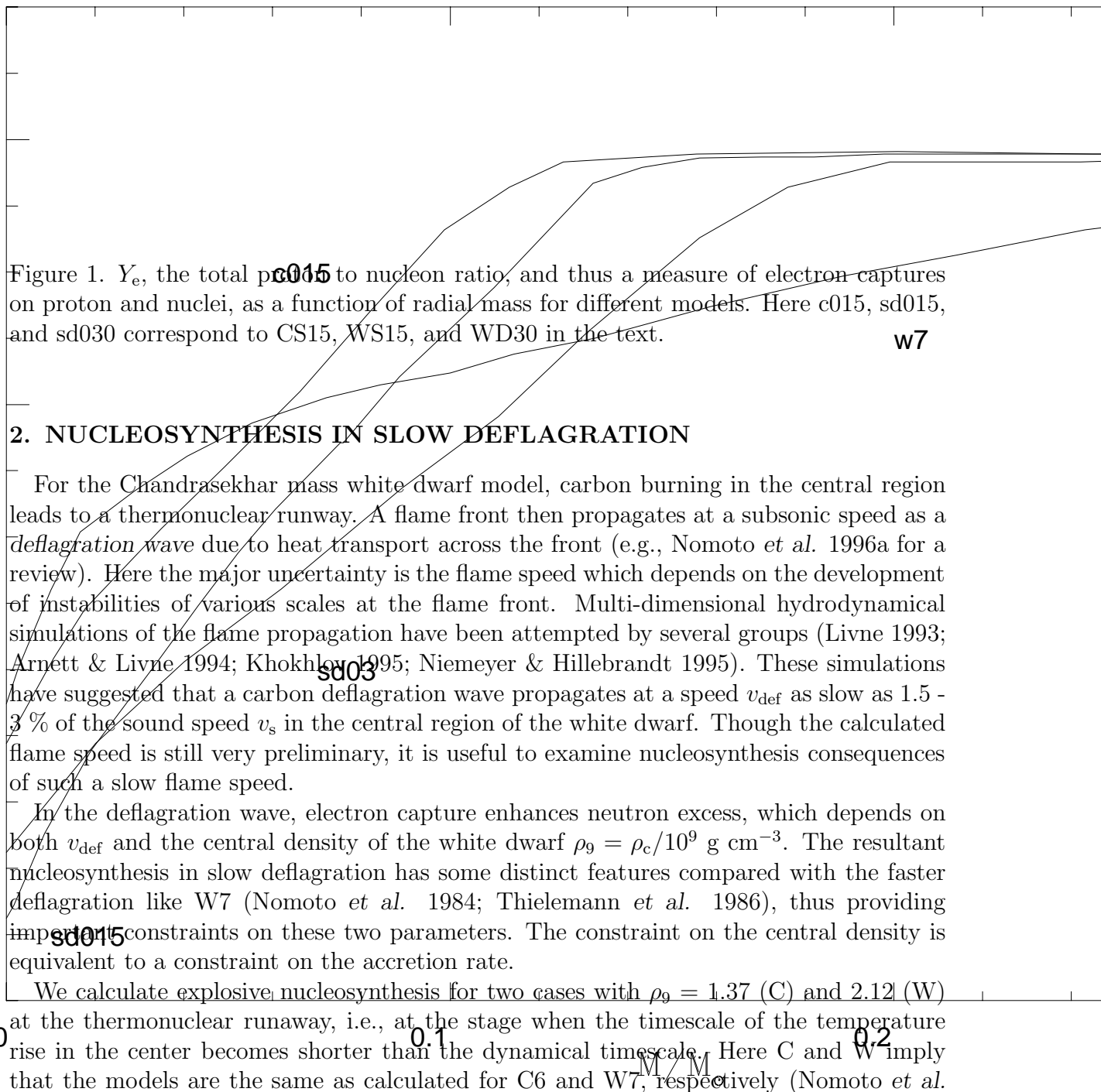
^cNational Astronomical Observatory, Mitaka, Tokyo 181

Among the major uncertainties involved in the Chandrasekhar mass models for Type Ia supernovae are the companion star of the accreting white dwarf (or the accretion rate that determines the carbon ignition density) and the flame speed after ignition. We present nucleosynthesis results from relatively slow deflagration (1.5 - 3 % of the sound speed) to constrain the rate of accretion from the companion star. Because of electron capture, a significant amount of neutron-rich species such as ^{54}Cr , ^{50}Ti , ^{58}Fe , ^{62}Ni , etc. are synthesized in the central region. To avoid the too large ratios of $^{54}\text{Cr}/^{56}\text{Fe}$ and $^{50}\text{Ti}/^{56}\text{Fe}$, the central density of the white dwarf at thermonuclear runaway must be as low as $\lesssim 2 \times 10^9 \text{ g cm}^{-3}$. Such a low central density can be realized by the accretion as fast as $\dot{M} \gtrsim 1 \times 10^{-7} M_{\odot} \text{ yr}^{-1}$. These rapidly accreting white dwarfs might correspond to the super-soft X-ray sources.

1. INTRODUCTION

Supernovae of different types have different progenitors, thus producing different heavy elements on different time scales during the chemical evolution of galaxies. Because the lifetime of their massive progenitors is about 10^{6-7} years being much shorter than the age of galaxies, Type II supernovae (SNe II) and Type Ib/Ic supernovae (SNe Ib/Ic) cause the heavy-element enrichment in the early phase of the galactic evolution.

In contrast, Type Ia supernovae (SNe Ia) produce heavy elements on a much longer time scale in the later phase of the galactic evolution. There are strong observational and theoretical indications that SNe Ia are thermonuclear explosions of accreting white dwarfs (e.g., Nomoto *et al.* 1994 for a review). However, the exact binary evolution that leads to SNe Ia has not been identified (e.g., Renzini 1996; Branch *et al.* 1995 for recent reviews). The identification of the progenitor's evolution is critically important 1) for clarifying whether the nature of SNe Ia at high redshift is the same as nearby SNe Ia, and 2) for understanding the origin of some systematic variations of light curves (i.e., brighter-slower), which is a critical material for the determination of cosmological parameters, H_0 and q_0 . In this paper, we provide some important constraints on the progenitor system from the viewpoint of nucleosynthesis, namely, the carbon ignition density which is translated into the accretion rate for the Chandrasekhar mass models.



2. NUCLEOSYNTHESIS IN SLOW DEFLAGRATION

For the Chandrasekhar mass white dwarf model, carbon burning in the central region leads to a thermonuclear runaway. A flame front then propagates at a subsonic speed as a *deflagration wave* due to heat transport across the front (e.g., Nomoto *et al.* 1996a for a review). Here the major uncertainty is the flame speed which depends on the development of instabilities of various scales at the flame front. Multi-dimensional hydrodynamical simulations of the flame propagation have been attempted by several groups (Livne 1993; Arnett & Livne 1994; Khokhlov 1995; Niemeyer & Hillebrandt 1995). These simulations have suggested that a carbon deflagration wave propagates at a speed v_{def} as slow as 1.5 - 3 % of the sound speed v_s in the central region of the white dwarf. Though the calculated flame speed is still very preliminary, it is useful to examine nucleosynthesis consequences of such a slow flame speed.

In the deflagration wave, electron capture enhances neutron excess, which depends on both v_{def} and the central density of the white dwarf $\rho_9 = \rho_c/10^9 \text{ g cm}^{-3}$. The resultant nucleosynthesis in slow deflagration has some distinct features compared with the faster deflagration like W7 (Nomoto *et al.* 1984; Thielemann *et al.* 1986), thus providing important constraints on these two parameters. The constraint on the central density is equivalent to a constraint on the accretion rate.

We calculate explosive nucleosynthesis for two cases with $\rho_9 = 1.37$ (C) and 2.12 (W) at the thermonuclear runaway, i.e., at the stage when the timescale of the temperature rise in the center becomes shorter than the dynamical timescale. Here C and W imply that the models are the same as calculated for C6 and W7, respectively (Nomoto *et al.*

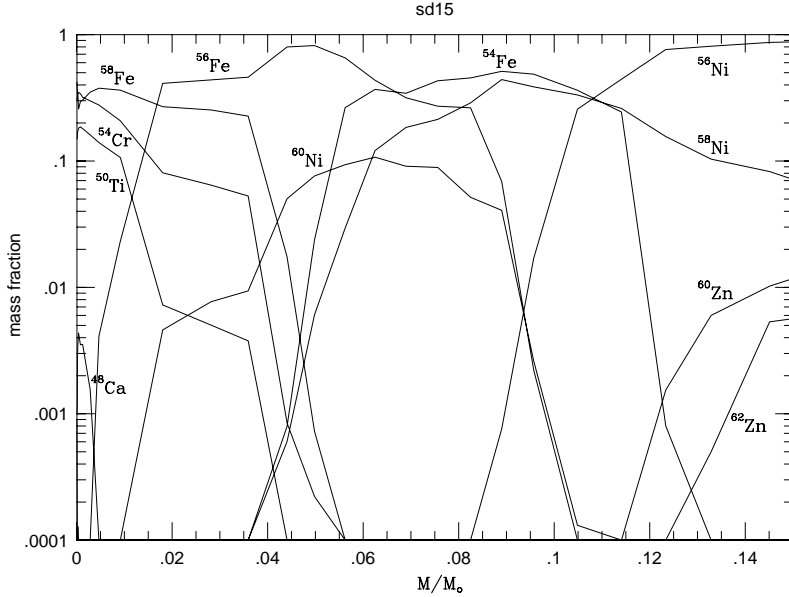


Figure 2. The abundance distribution in slow deflagration WS15.

1984). For the slow (S) deflagration, we adopt $v_{\text{def}}/v_s = 0.015$ (WS15, CS15) and 0.03 (WS30). The central region behind the slower deflagration undergoes electron capture for a longer time than in W7, thereby having significantly reduced Y_e . In Figure 1, profiles of Y_e for these cases and W7 are shown (Thielemann *et al.* 1996b). In general it can be recognized that small burning front velocities lead to steep Y_e -gradient which flatten with increasing velocities. Lower central ignition densities shift the curves up (CS15), but the gradient is the same for the same propagation speed.

Figure 2 shows the abundance distribution of neutron-rich species such as ^{54}Cr , ^{50}Ti , ^{58}Fe , and ^{62}Ni behind the slow deflagration for WS15. The locations of ^{54}Fe and ^{58}Ni , overproduced in W7, correspond to $Y_e = 0.47\text{-}0.485$. Due to the Y_e -gradients which are steeper than for W7, the amount of matter in a given Y_e -range is reduced, but also smaller central values are attained, giving rise to more neutron-rich nuclei. $Y_e \sim 0.46 \approx 26/56$ leads to a large abundance of stable ^{56}Fe (not from ^{56}Ni decay). $Y_e = 0.44 - 0.46$ result also in ^{48}Ca , ^{50}Ti , ^{54}Cr , and ^{58}Fe . Of these nuclei ^{48}Ca with $Z/A \approx 0.42$ is only produced if Y_e approaches values close to and smaller than 0.44 (Woosley 1996; Meyer *et al.* 1996). As the deflagration wave propagates outwards, the white dwarf gradually expands to undergo less electron capture and thus mostly ^{56}Ni is synthesized. Eventually, the deflagration enters the region of incomplete Si burning and explosive O-Ne-C burning.

The neutron excess is sensitive to the initial central density. For WS15 ($\rho_9 = 2.12$), the masses of ^{54}Cr and ^{50}Ti are smaller than those for CS15 ($\rho_9 = 1.37$) by a factor of ~ 5 and 20, respectively, and those for WS30 ($v_{\text{def}}/v_s = 0.03$) by a factor of 2 and 4, respectively.

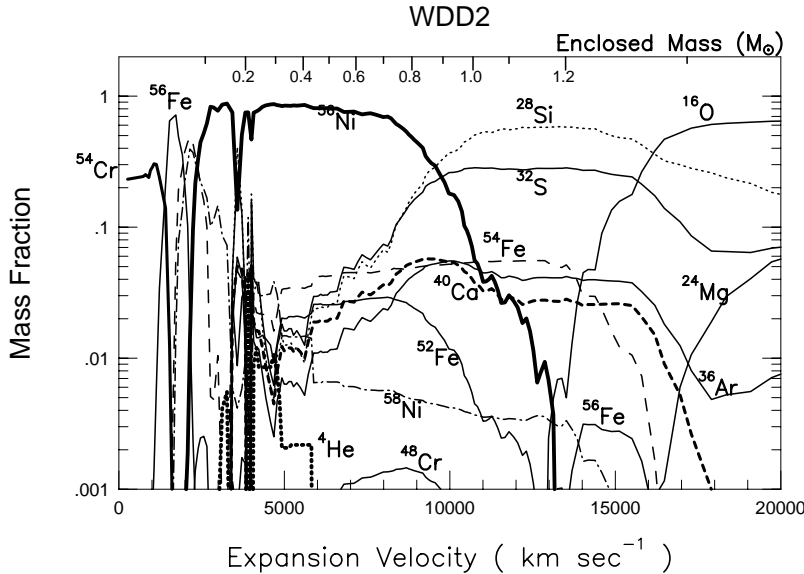


Figure 3. The abundance distribution in the delayed detonation model WDD2 as a function of interior mass and the expansion velocity.

3. NUCLEOSYNTHESIS IN DELAYED DETONATION

If the deflagration speed continues to be much slower than in W7, the white dwarf undergoes strong pulsation as first found by Nomoto *et al.* (1976). In this *pulsating deflagration* model, the white dwarf expands to quench nuclear burning when the total energy of the star is still negative. Then the star contracts to burn more material to make the total energy positive ($\sim 5 \times 10^{49}$ erg s $^{-1}$).

The deflagration might induce a detonation at low density layers. In the *delayed detonation* model (Khokhlov 1991a; Woosley & Weaver 1994), the deflagration wave is assumed to be transformed into detonation at a certain layer during the first expansion phase. In the *pulsating* delayed detonation model (Khokhlov 1991b), the transition into detonation is assumed to occur near the maximum compression due to mixing.

We study explosive nucleosynthesis with a large reaction network (Thielemann *et al.* 1996) for various delayed detonation (DD) models, which has not been discussed in detail before (Nomoto *et al.* 1996b). We artificially transform the slow deflagration WS15 into detonation when the density ahead of the flame decreases to 3.0 , 2.2 , and 1.7×10^7 g cm $^{-3}$ (WDD3, WDD2, and WDD1, respectively, where 3, 2, and 1 indicate ρ_7 at the transition). Then the carbon detonation propagates through the layers with $\rho < 10^8$ g cm $^{-3}$. The explosion energy of three WDD models is 1.5×10^{51} ergs s $^{-1}$ and the mass of ^{56}Ni is $0.73 M_{\odot}$ (WDD3), $0.58 M_{\odot}$ (WDD2), and $0.45 M_{\odot}$ (WDD1).

Figure 3 shows the abundance distribution against the expansion velocity and M_r after the passage of the slow deflagration (WS15) and the delayed detonation. For comparison, the abundance distribution of W70 is shown in Figure 4, where the initial metallicity (i.e., the initial CNO elements which are later transformed into ^{22}Ne) is assumed to be zero.

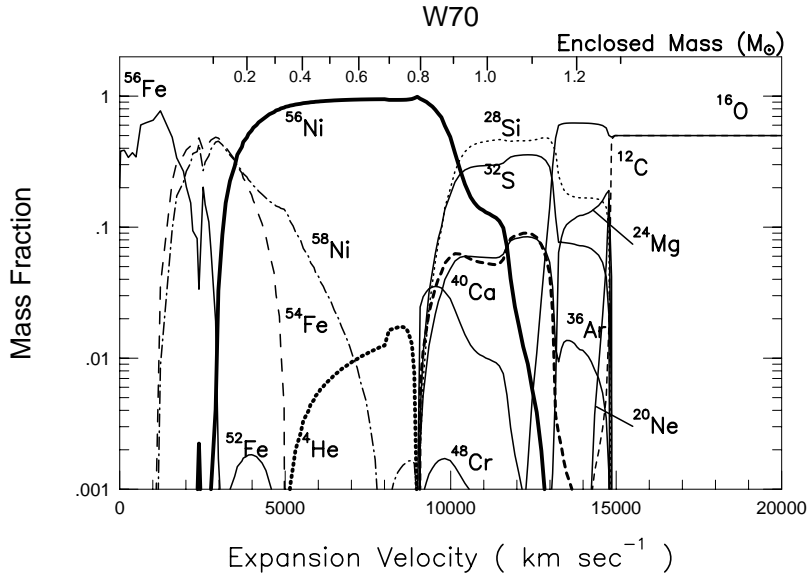


Figure 4. The abundance distribution in the delayed detonation model W70 as a function of interior mass and the expansion velocity.

It is seen that WDD2 and WDD1 produce two Si-S-Ar peaks at low velocity (~ 4000 km s^{-1}) and high velocities ($10,000 - 15,000$ km s^{-1}). The low velocity intermediate mass elements are important to observe at late times to distinguish models. In particular, the minimum velocity of Ca in WDD models is ~ 4000 km s^{-1} , which should be compared with the observed minimum velocities of Ca indicated by the red edge of the Ca II H and K absorption blend (Fisher *et al.* 1995).

Meikle *et al.* (1996) have observed a P Cyg-like feature at $\sim 1.05/1.08$ μm in SN 1994D and 1991T. They note that, if this feature is due to He, He in SN 1994D is likely to be formed in α -rich freezeout and mixed out to the high velocity layers ($\sim 12,000$ km s^{-1}). The maximum velocity of He is $5000 - 6000$ km s^{-1} in WDDs being slower than ~ 9000 km s^{-1} in W7, so that more extensive mixing of He would be required for WDDs than W7. Alternatively, if the feature is due to Mg, the Mg velocity is confined in $12,500 - 16,000$ km s^{-1} in SN 1994D, which is consistent with W7 ($13,000 - 15,000$ km s^{-1}). For WDDs, on the other hand, the minimum velocities of Mg are $14,500$ km s^{-1} (WDD1), $16,500$ km s^{-1} (WDD2), and $18,000$ km s^{-1} (WDD3), and the latter two models seem to have too high velocities.

4. YIELDS OF TYPE IA SUPERNOVAE

Total isotopic compositions of WDD1 - WDD3 are given in Table 1, and compared with the solar abundances in Figure 5 which are normalized to ^{56}Fe . Table 1 also includes W7 and W70 updated with the latest reaction rates along with W70 (Thielemann *et al.* 1996b). We note:

- 1) The synthesized amounts of Fe and thus the ratio between the intermediate mass

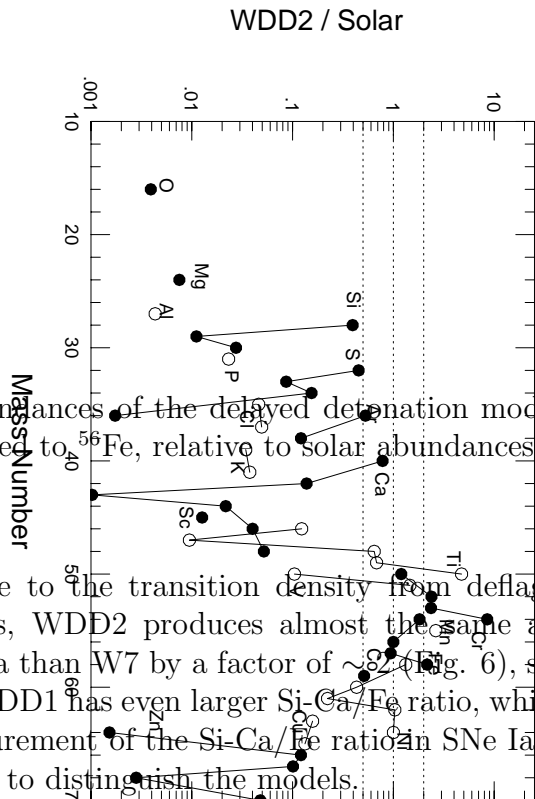


Figure 5. The ratios of integrated abundances of the delayed detonation model WDD2 after decay of unstable nuclei, normalized to ^{56}Fe , relative to solar abundances.

elements to Fe, Si-Ca/Fe, are sensitive to the transition density from deflagration to detonation. Among the WDD models, WDD2 produces almost the same amount of ^{56}Ni as W7 ($\sim 0.6 M_{\odot}$) but more Si-Ca than W7 by a factor of ~ 82 (Fig. 6), since more oxygen is burned in the outer layers. WDD1 has even larger Si-Ca/Fe ratio, which is close to the solar ratio. Therefore, the measurement of the Si-Ca/Fe ratio in SNe Ia remnants (Tycho, SN 1006, etc.) would be useful to distinguish the models.

2) Some neutron-rich species such as ^{54}Cr and ^{50}Ti are overproduced with respect to ^{56}Fe . To see the degree of overproduction, we combine nucleosynthesis products of SNe Ia and SNe II with various ratios and compare with solar abundances of heavy elements and their isotopes.

Nucleosynthesis products of SNe II as a function of stellar masses are taken from the calculations by Nomoto & Hashimoto (1988), Hashimoto *et al.* (1989, 1996) and Thielemann *et al.* (1996a) as summarized in Tsujimoto *et al.* (1995). SNe II yields integrated over $m_l = 10 M_{\odot}$ to $m_u = 50 M_{\odot}$ with the Salpeter IMF are given in Table 1. The upper mass bound m_u is chosen to give $[\text{O}/\text{Fe}] = +0.4$, which is consistent with the observations of low metallicity stars for $[\text{Fe}/\text{H}] < -1$.

Nucleosynthesis products of SNe Ia are those from WDD2 and W70, and the results are shown in Figures 6 - 7. For WDD2, the best fit to the solar abundances are obtained for the ratio between SNe Ia and SNe II contributions as $r = 0.07$ where r is the mass fraction contributed by SNe Ia per unit mass of all heavy elements in the gas as defined in Tsujimoto *et al.* (1995).

Aided with a reasonable chemical evolution model (Yoshii *et al.* 1996), the number of SNe Ia ever occurred relative to SNe II is determined to be $N_{\text{Ia}}/N_{\text{II}} = 0.12$ in order to reproduce the observed abundances. This is consistent with the fact that the observed estimate of SNe Ia frequency is as low as 10 % of the total supernova occurrence (van den

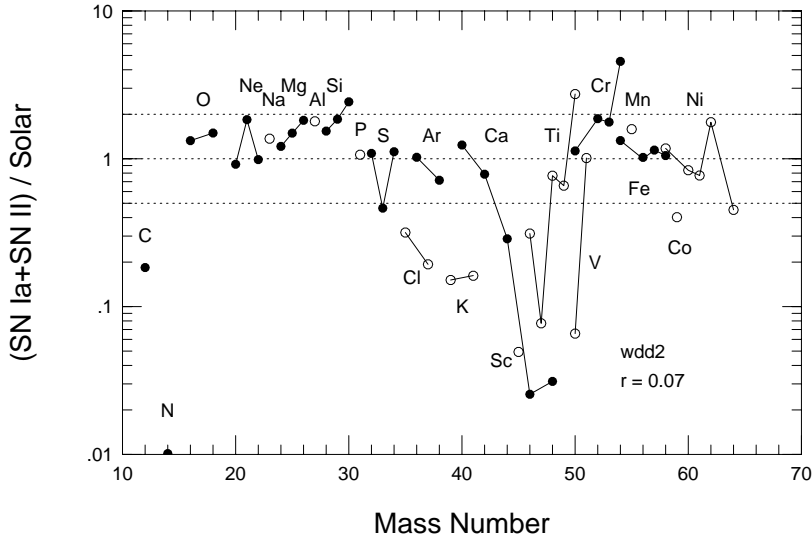


Figure 6. Solar abundance pattern based on synthesized heavy elements from a composite of Type Ia and Type II supernova explosions with the most probable ratio of r . Relative abundances of synthesized heavy elements and their isotopes normalized to the corresponding solar abundances are shown by circles. Here WDD2 is adopted for the Type Ia supernova model.

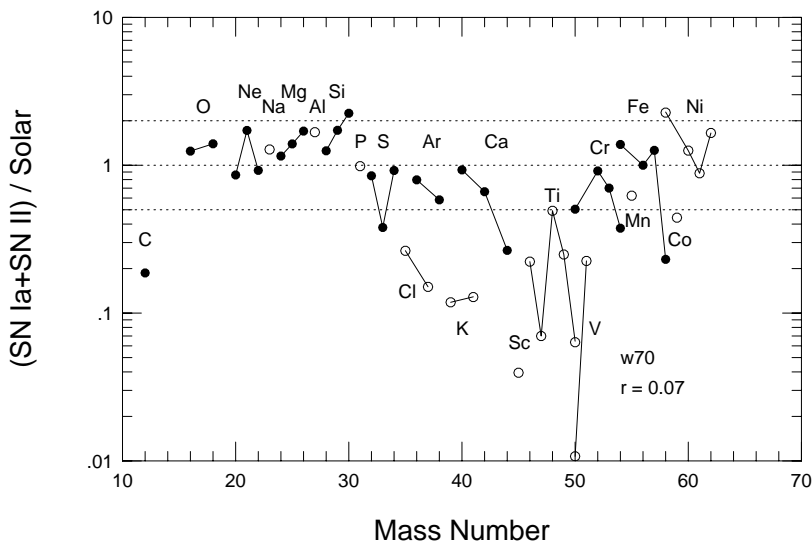


Figure 7. Same as Figure 6 but for W70 as an SN Ia model.

Bergh & Tammann 1991; Tsujimoto *et al.* 1995).

With this relative frequency, ^{56}Fe from SNe Ia is about 50 % of total ^{56}Fe . Then the abundance ratios between neutron-rich species and ^{56}Fe could be reduced by a factor of ~ 2 . For W70, the excess of $^{58}\text{Ni}/^{56}\text{Fe}$ is now within the uncertainties (Fig. 7). For WDDs, on the other hand, ^{54}Cr and ^{50}Ti are overproduced as seen in Figure 6 even when the contribution from SNe II is taken into account.

The above results imply that the central density of the Chandrasekhar mass white dwarf at thermonuclear runaway must be as low as $\lesssim 2 \times 10^9 \text{ g cm}^{-3}$, though the exact constraint depends somewhat on the flame speed. Such a low central density can be realized by the accretion as fast as $\dot{M} > 1 \times 10^{-7} M_{\odot} \text{ yr}^{-1}$. Such rapidly accreting white dwarfs might correspond to the super-soft X-ray sources.

Acknowledgements

This work has been supported in part by the grant-in-Aid for Scientific Research (05242102, 06233101, 4227) and COE research (07CE2002) of the Ministry of Education, Science, and Culture in Japan, and the Swiss Nationalfonds.

REFERENCES

1. Arnett, W.D. & Livne, E. 1994, ApJ 427, 314
2. Branch, D., Livio, M., Yungelson, L.R., Boffi, F.R., & Baron, E. 1995, PASP 107, 717
3. Fisher, A., Branch, D., Höflich, P., & Khokhlov, A. 1995, ApJ 447, L73
4. Hashimoto, M., Nomoto, K., & Thielemann, F.-K. 1989, A&A 210, L5
5. Hashimoto, M., Nomoto, K., Tsujimoto, T., & Thielemann, F.-K. 1996, in IAU Colloquium 145, Supernovae and Supernova Remnants, ed. R. McCray & Z. Wang (Cambridge University Press), p. 157
6. Khokhlov, A.M. 1991a, A&A 245, 114
7. Khokhlov, A.M. 1991b, A&A 245, L25
8. Khokhlov, A.M. 1995, ApJ 449, 695
9. Livne, E. 1993, ApJ 406, L17
10. Meikle, W.P.W. *et al.* 1996, MN in press
11. Meyer, B.S., Krishnan, T.D., & Clayton, D.D. 1996, ApJ 462, 825
12. Niemeyer J.C., & Hillebrandt W. 1995, ApJ 452, 769
13. Nomoto, K. 1982, ApJ 253, 798
14. Nomoto, K., & Hashimoto, M. 1988, Phys. Rep. 163, 13
15. Nomoto, K., & Kondo, Y. 1991, ApJ 367, L19
16. Nomoto, K., Sugimoto, D., & Neo, S. 1976, ApSS 39, L37
17. Nomoto, K., Thielemann, F.-K., & Yokoi, K. 1984, ApJ 286, 644
18. Nomoto, K., Yamaoka, H., Shigeyama, T., Kumagai, S., & Tsujimoto, T. 1994, in Supernovae (Les Houches, Session LIV), ed. S. Bludman *et al.* (Elsevier Sci. Publ.), p. 199
19. Nomoto, K., Yamaoka, H., Shigeyama, T., & Iwamoto, K. 1996a, in IAU Colloquium 145, Supernovae and Supernova Remnants, ed. R. McCray & Z. Wang (Cambridge University Press), p. 49
20. Nomoto, K., Iwamoto, K., Nakasato, N., Thielemann, F.-K., Brachwitz, F., Young,

- T., Shigeyama, T., Tsujimoto, T., & Yoshii, Y. 1996b, in *Thermonuclear Supernovae*, ed. R. Canal *et al.* (NATO ASI, Kluwer), in press
21. Renzini, A. 1996, in *IAU Colloquium 145, Supernovae and Supernova Remnants*, ed. R. McCray & Z. Wang (Cambridge University Press), p. 77
22. Thielemann, F.-K., Nomoto, K., & Yokoi, K. 1986, *A&A* 158, 17
23. Thielemann, F.-K., Nomoto, K., & Hashimoto, M. 1996a, *ApJ* 460, 408
24. Thielemann, F.-K., Nomoto, K., Iwamoto, K., & Brachwitz, F. 1996b, in *Thermonuclear Supernovae*, ed. R. Canal *et al.* (NATO ASI, Kluwer), in press
25. Tsujimoto, T., Nomoto, K., Yoshii, Y., Hashimoto, M., Yanagida, S., & Thielemann, F.-K., 1995, *MN* 277, 945
26. van den Bergh, S., & Tammann, G. 1991, *ARA&A* 29, 363
27. Woosley, S.E. 1996, preprint
28. Woosley, S.E., & Weaver, T.A. 1994, in *Supernovae (Les Houches, Session LIV)*, ed. J. Audouze *et al.* (Elsevier Sci. Publ.) p. 63
29. Yoshii, Y., Tsujimoto, T., & Nomoto, K. 1996, *ApJ* 462, 266

Table 1
Nucleosynthesis products of SN II and Ia

Species	Synthesized mass (M_{\odot})					
	Type II 10~50 M_{\odot}	W70	W7	Type Ia WDD1	WDD2	WDD3
¹² C	7.93E-02	5.08E-02	4.83E-02	1.80E-03	1.15E-03	5.82E-04
¹³ C	3.80E-09	1.56E-09	1.40E-06	3.52E-08	1.04E-08	6.90E-09
¹⁴ N	1.56E-03	3.31E-08	1.16E-06	3.08E-04	2.44E-04	7.42E-05
¹⁵ N	1.66E-08	4.13E-07	1.32E-09	6.84E-07	2.75E-07	1.68E-07
¹⁶ O	1.80	1.33E-01	1.43E-01	9.96E-02	6.93E-02	4.69E-02
¹⁷ O	9.88E-08	3.33E-10	3.54E-08	3.99E-06	4.50E-06	1.72E-06
¹⁸ O	4.61E-03	2.69E-10	8.25E-10	6.96E-07	4.62E-07	2.42E-07
¹⁹ F	1.16E-09	1.37E-10	5.67E-10	1.68E-09	8.90E-10	5.48E-10
²⁰ Ne	2.12E-01	2.29E-03	2.02E-03	1.45E-03	9.13E-04	6.77E-04
²¹ Ne	1.08E-03	2.81E-08	8.46E-06	4.09E-06	1.47E-06	2.30E-06
²² Ne	1.83E-02	2.15E-08	2.49E-03	1.34E-05	1.96E-06	1.39E-06
²³ Na	6.51E-03	1.41E-05	6.32E-05	3.20E-05	1.30E-05	6.53E-06
²⁴ Mg	8.83E-02	1.58E-02	8.50E-03	8.29E-03	4.76E-03	2.93E-03
²⁵ Mg	1.44E-02	1.64E-07	4.05E-05	4.60E-05	2.39E-05	1.44E-05
²⁶ Mg	2.01E-02	1.87E-07	3.18E-05	5.52E-05	3.57E-05	1.09E-05
²⁷ Al	1.48E-02	1.13E-04	9.86E-04	4.65E-04	2.74E-04	1.73E-04
²⁸ Si	1.05E-01	1.38E-01	1.50E-01	3.48E-01	2.71E-01	2.04E-01
²⁹ Si	8.99E-03	6.03E-05	8.61E-04	6.05E-04	3.87E-04	2.49E-04
³⁰ Si	8.05E-03	3.09E-05	1.74E-03	1.07E-03	6.35E-04	3.94E-04
³¹ P	1.21E-03	8.51E-05	4.18E-04	2.67E-04	1.80E-04	1.23E-04
³² S	3.84E-02	9.19E-02	8.41E-02	2.09E-01	1.65E-01	1.24E-01
³³ S	1.78E-04	5.83E-05	4.50E-04	3.48E-04	2.49E-04	1.74E-04

Species	Synthesized mass (M_{\odot})					
	Type II	Type Ia				
	10~50 M_{\odot}	W70	W7	WDD1	WDD2	WDD3
³⁴ S	2.62E-03	2.84E-06	1.90E-03	3.42E-03	2.50E-03	1.75E-03
³⁶ S	1.78E-06	1.09E-11	3.15E-07	2.29E-07	1.33E-07	8.58E-08
³⁵ Cl	1.01E-04	8.06E-06	1.34E-04	1.21E-04	9.83E-05	7.67E-05
³⁷ Cl	1.88E-05	5.36E-06	3.98E-05	4.23E-05	3.36E-05	2.52E-05
³⁶ Ar	6.62E-03	1.99E-02	1.49E-02	4.12E-02	3.35E-02	2.50E-02
³⁸ Ar	1.37E-03	5.93E-07	1.06E-03	1.71E-03	1.45E-03	1.12E-03
⁴⁰ Ar	2.27E-08	1.14E-12	1.26E-08	8.16E-09	6.08E-09	4.53E-09
³⁹ K	6.23E-05	1.82E-06	8.52E-05	1.05E-04	9.00E-05	7.00E-05
⁴¹ K	5.07E-06	5.33E-07	7.44E-06	8.39E-06	7.12E-06	5.53E-06
⁴⁰ Ca	5.77E-03	1.95E-02	1.23E-02	4.07E-02	3.45E-02	2.58E-02
⁴² Ca	4.23E-05	1.55E-08	3.52E-05	4.69E-05	4.06E-05	3.24E-05
⁴³ Ca	1.08E-06	6.81E-08	1.03E-07	6.97E-08	6.31E-08	4.73E-08
⁴⁴ Ca	5.53E-05	1.55E-05	8.86E-06	2.06E-05	2.07E-05	1.42E-05
⁴⁶ Ca	1.43E-10	5.88E-11	1.99E-09	6.17E-08	7.18E-08	3.00E-08
⁴⁸ Ca	5.33E-14	5.96E-12	7.10E-12	4.21E-06	4.41E-06	3.62E-06
⁴⁵ Sc	2.29E-07	3.92E-08	2.47E-07	3.54E-07	3.23E-07	2.51E-07
⁴⁶ Ti	7.48E-06	7.87E-07	1.71E-05	2.06E-05	1.76E-05	1.44E-05
⁴⁷ Ti	2.11E-06	7.49E-07	6.04E-07	1.21E-06	1.24E-06	7.40E-07
⁴⁸ Ti	1.16E-04	3.21E-04	2.03E-04	8.17E-04	8.53E-04	6.76E-04
⁴⁹ Ti	5.98E-06	1.64E-06	1.69E-05	6.55E-05	6.71E-05	5.24E-05
⁵⁰ Ti	3.81E-10	1.14E-05	1.26E-05	4.57E-04	4.60E-04	4.80E-04
⁵⁰ V	7.25E-10	5.66E-09	8.28E-09	5.49E-08	5.69E-08	4.52E-08
⁵¹ V	1.00E-05	2.10E-05	5.15E-05	2.92E-04	3.18E-04	2.10E-04
⁵⁰ Cr	4.64E-05	7.61E-05	2.71E-04	5.86E-04	5.24E-04	3.98E-04
⁵² Cr	1.15E-03	6.63E-03	5.15E-03	1.75E-02	2.01E-02	1.67E-02
⁵³ Cr	1.19E-04	4.65E-04	7.85E-04	2.02E-03	2.26E-03	1.87E-03
⁵⁴ Cr	2.33E-08	1.79E-04	1.90E-04	2.03E-03	2.03E-03	2.08E-03
⁵⁵ Mn	3.86E-04	6.27E-03	8.23E-03	1.57E-02	1.88E-02	1.44E-02
⁵⁴ Fe	3.62E-03	8.18E-02	1.04E-01	7.26E-02	7.08E-02	6.29E-02
⁵⁶ Fe	8.44E-02	6.72E-01	6.13E-01	4.56E-01	6.15E-01	7.62E-01
⁵⁷ Fe	2.72E-03	1.98E-02	2.55E-02	1.03E-02	1.39E-02	1.94E-02
⁵⁸ Fe	7.22E-09	9.34E-04	9.63E-04	4.09E-03	4.06E-03	4.10E-03
⁵⁹ Co	7.27E-05	6.28E-08	1.02E-03	6.83E-04	8.60E-04	1.12E-03
⁵⁸ Ni	3.63E-03	9.67E-02	1.28E-01	3.01E-02	3.34E-02	4.62E-02
⁶⁰ Ni	1.75E-03	1.43E-02	1.05E-02	4.03E-03	4.15E-03	4.78E-03
⁶¹ Ni	8.35E-05	2.30E-04	2.51E-04	7.93E-05	9.23E-05	1.17E-04
⁶² Ni	5.09E-04	1.37E-03	2.66E-03	1.26E-03	1.36E-03	1.88E-03
⁶⁴ Ni	3.20E-14	1.22E-06	1.31E-06	3.45E-04	3.35E-04	3.61E-04
⁶³ Cu	8.37E-07	2.86E-06	1.79E-06	3.91E-05	4.25E-05	3.49E-05
⁶⁵ Cu	4.07E-07	9.60E-07	6.83E-07	1.48E-05	1.59E-05	1.00E-05
⁶⁴ Zn	1.03E-05	1.05E-04	1.22E-05	3.54E-07	6.97E-07	2.56E-06
⁶⁶ Zn	8.61E-06	8.65E-06	2.12E-05	3.15E-05	3.18E-05	3.74E-05
⁶⁷ Zn	1.52E-08	3.96E-09	1.34E-08	3.55E-06	3.90E-06	1.98E-06
⁶⁸ Zn	3.92E-09	3.29E-09	1.02E-08	4.38E-07	4.94E-07	2.81E-07